Results in Engineering 11 (2021) 100248

Contents lists available at ScienceDirect

Results in Engineering

journal homepage: www.sciencedirect.com/journal/results-in-engineering

Mineralogical and physical studies of low-grade tantalum-tin ores from selected areas of Rwanda

Jean Baptiste Habinshuti [a,b,*], Jeanne Pauline Munganyinka [a,b], Adelena R. Adetunji [a,c], Brajendra Mishra [b], Grace Ofori-Sarpong [d], Gbetoglo Charles Komadja [a], Himanshu Tanvar [b], Janvier Mukiza [e], Azikiwe P. Onwualu [a]

[a] Department of Materials Science and Engineering, African University of Science and Technology, Abuja, Nigeria
[b] Department of Mechanical Engineering, Worcester Polytechnic Institute, 100 Institute Road, Worcester, MA 01609, USA
[c] Department of Materials Science and Engineering, Obafemi Awolowo University, Ile-Ife, Nigeria
[d] University of Mines and Technology, Tarkwa, Ghana
[e] School of Education, College of Education, University of Rwanda, P.O. BOX 55, Rwamagana, Rwanda

ARTICLE INFO

Keywords:
Tantalum
Columbite
Cassiterite
Ores
Beneficiation
Mineralogical compositions

ABSTRACT

In this work, mineralogical and physical characterization of low-grade tantalum-tin ore-samples from Ntunga and Kamonyi of Rwanda were carried out using various techniques. The ore-samples were classified as low-grade and non-radioactive ores as they contained less than 0.1% Ta_2O_5 and Nb_2O_5, and the percentage of radioactive oxides were below the critical value of 0.5%. The characteristic elements associated with tantalum as detected and quantified by Inductively Coupled Plasma-Optical Emission Spectroscopy and expressed as oxides for their natural occurrence included Ta_2O_5, Nb_2O_5, Fe_2O_3, MnO, SnO_2, MgO, TiO_2, U_3O_8, and ThO_2, among others. Analysis of samples in raw form showed presence of valuable minerals of cassiterite (0.067%–0.469%), and columbite-(Fe) with Nb_2O_5 (0.050%–0.062%) and Fe_2O_3 (0.194%–0.769%), and tantalite-(Mn) with Ta_2O_5 (0.039%–0.063%) and MnO (0.080%–0.186%). Upon a rough gravity concentration, the ore-samples resulted in concentrate with compositions of 66.14%SnO_2, 7.66%Ta_2O_5 and 7.70%Nb_2O_5. These minerals with most particle sizes of 125 μm were disseminated within the alumino-silicate matrix of the pegmatite rock. All samples showed nearly similar mineralogical compositions, and the XRD results strongly supported this observation, with diffractograms showing identical characteristic peaks which matched mainly with kaolinite, muscovite, and quartz minerals. Peaks of cassiterite, columbite and tantalite were not strong and visible but upon concentration, they became clear, sharp, and strong. These results will serve as a baseline for selecting and designing appropriate processing technique to effectively harness this mineral resource.

1. Introduction

Tantalum (Ta) is a transition metal element of high economic importance due to its rising demand for technological applications [1,2]. The unique properties of Ta such as high dielectric constant, the stability of its oxides and corrosion resistance [3–5] make this metal attractive in the field of electronics, aerospace, nuclear and automobile industries, military and medicine [2,6,7]. The metal, tantalum is always associated with niobium and both are recovered mainly from columbite-tantalite group minerals which are present as minor components in both primary granites, granitic pegmatites and greisen rocks [1]. Tantalum and niobium are also known to occur in tin-bearing ore-deposits and have been concentrated and successfully extracted from the tin slags disposed as an industrial waste from cassiterite smelting processes [8–10]. The secondary deposits resulting from the strong weathering and erosion processes acting on the primary tantalum-tin bearing rocks, form a weathered rock that hosts an appreciable amount of tantalum and tin minerals [11,12]. Tantalum-tin containing mineral is one of the highly valuable and unexploited mineral resources in Africa, but lack of technology for exploration, beneficiation and extraction to efficiently harness the potential of this resource, make it impossible for it to contribute to the wealth of Africa [5,12].

In nature, tantalum co-exists with niobium as oxides associated with oxides of iron and manganese. The association may include tin,

* Corresponding author. Department of Materials Science and Engineering, African University of Science and Technology, Abuja, Nigeria.
E-mail address: hbaptiste@aust.edu.ng (J.B. Habinshuti).

https://doi.org/10.1016/j.rineng.2021.100248
Received 7 June 2021; Accepted 30 June 2021
Available online 4 July 2021

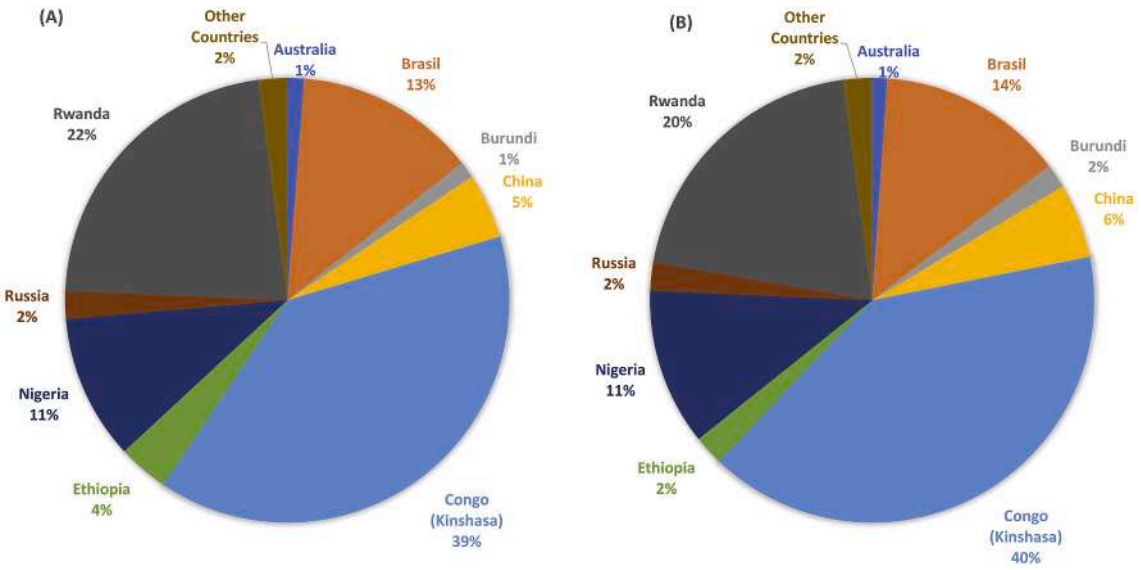

Fig. 1. Global tantalum mines production (A) 2018 and (B) 2019 [9].

titanium, lithium, cesium, and trace amounts of tungsten, uranium, and thorium in pegmatites rocks and other related lithologies [13,14]. Tantalum and niobium have a strong coherence in geochemical behaviors, and are always closely associated and freely substitute each other in the same type of mineral deposits [15,16]. The main reason for such coherence is the ionic potential associated with their identical ionic radii and valency states [15]. This gives them a high ionic charge-to-ionic radius ratio, which makes them lithophilic elements with a strong affinity to oxygen and high concentration in silicates of the earth's crust [15,16]. Columbite-tantalite group minerals [$(Fe,Mn)O(Ta,Nb)_2O_5$] are major sources for production of tantalum and niobium. The group include [tantalite-(Fe) or tantalite-(Mn)] and [columbite-(Fe) or columbite-(Mn)] [2,17]. Tantalum, tin and niobium also exist in other types of minerals such as pyrochlore, ixiolite, wodginite as complex oxides and hydroxides minerals [14].

In Africa, the tantalum industry suffers from lack of smelting and processing plants to separate tantalum from niobium. These metals are thus sold together as concentrates of tantalum minerals but only the value of Ta_2O_5 contained is paid for. Tantalum and niobium are not traded on any metal exchange as there is no official price. The price is based on negotiations and contracts between the seller and the buyer [5,18]. Central African countries are major contributors to the global supply of tantalum concentrates (Fig. 1) and have been under international pressure resulting from tantalum's status as conflict mineral [19]. Rwanda has however shown good reputation for conflict-free policies and assuring reasonable mining practices [20].

Tantalite ores are mined and processed through several steps using different technologies for production of pure tantalum. Successful processing of minerals into various useful products is usually based on the understanding of the differences in the physical or chemical properties of various species present [21]. In this regard, a proper knowledge of the physico-chemical and mineralogical features of the tantalum-tin ores is required to come up with efficient and eco-friendly processing techniques. For instance, depending on the nature of the ore, the beneficiation process may include pre-concentration, primary concentration, and concentrate clean-up [22,23]. If the ore-sample contains less than 0.1%Ta_2O_5 and Nb_2O_5, its beneficiation starts with an enrichment step, which may involve a gravity separation [24]. If the concentrates indicate the presence of magnetically susceptible materials, its beneficiation proceeds with the removal of all magnetic compounds before the dissolution and leaching of the concentrate [25]. Similarly, when radioactive elements are present in the concentrate, they should also be removed before chemical leaching for separation of tantalum from niobium [23,25,26].

Musha-Ntunga and Kamonyi are well-known areas in Rwanda for production of cassiterite and tantalite concentrates. However, there is no significant work that has been done to characterize the low-grade tantalum-tin ores from these areas. In this study, physical studies of low-grade tantalum-tin ore-samples collected from two selected areas in Rwanda (Ntunga and Kamonyi) are reported. In addition, various characterization techniques such as scanning electron microscopy with energy-dispersive x-ray spectroscopy (SEM-EDS), inductively coupled plasma-optical emission spectroscopy (ICP-OES), X-ray diffraction (XRD), were used for deep understanding of their mineralogical and chemical characteristics. The nature and associated minerals of the ore are usually revealed through characterization studies. This in turn dictates the processing routes for the ore. This study is therefore intended to provide the baseline data for the selecting and designing the appropriate technique to effectively harness this mineral resource from the areas.

2. Experimental procedures

2.1. Materials sampling

Tantalum-tin ore samples used in this study were collected from two different active mines in Rwanda. The first three samples (**R–N1**, **R–N2**, **R–N3**) were collected in raw form from three different points (1°57′43″S 30°21′44″E, 1°57′45″S 30°21′45″E, 1°57′46″S 30°21′39″E) at Ntunga mine in the Eastern Province of Rwanda. Sample **R-KMY Raw** and its concentrate **R-KMNY-Con** were obtained from the Southern Province; Kamonyi, COMIKA mine concession (1°55′11.0″S 29°56′33.4″E). These areas have been known for their productions of cassiterite and tantalite ores in Rwanda. The concentrate as received had earlier been pre-concentrated on site by gravity separation. The sampling points were chosen based on known locations of veins in the mining area and sometimes particles of tantalite ore were visible with necked eye. Samples were collected at the surface of the mining pit or inside the shaft and sometimes where landslide occurred due to erosion.

2.2. Instrumentation

The particle size analysis of the ore sample was performed by using particle size analyzer, the Microtrac flowSync that uses two blue lasers for laser diffraction analysis (approx. 14 nm resolution) combined with

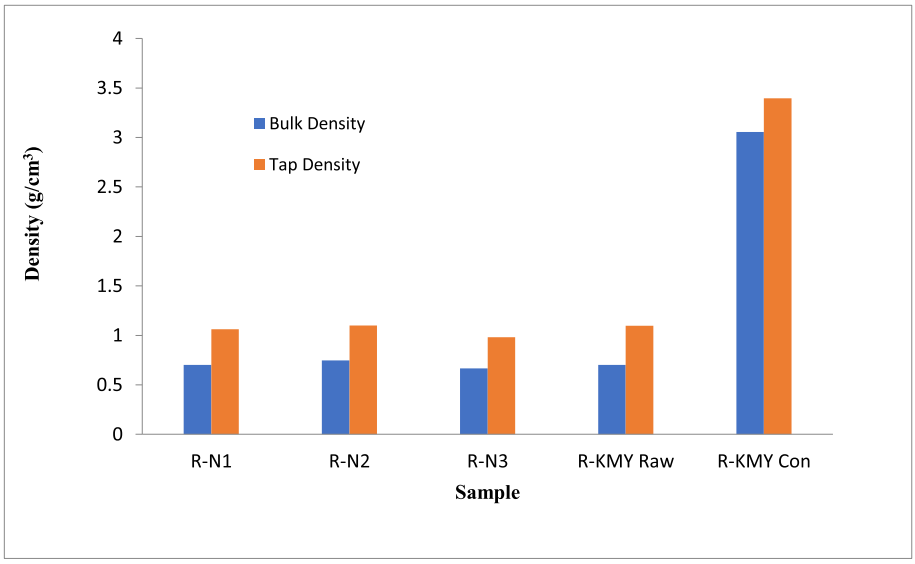

Fig. 2. Comparison between bulk and tap densities of investigated ore-samples.

2D image analysis to capture the particle size distribution data. The carrier fluid is deionized (DI) water with a refractive index of 1.33. The sample was prepared by adding the powder sample to a 1:100 dilution of Triton-X100, to allow particles integration into the DI water and micro-pipetted in until the loading factor was 0.950–0.956. The sample system (wet) operates at a flow rate of 55% and before introduction of the subsequent samples, the system is rinsed two times, and deaerated three times. The particles size with upper and lower edge is 2000 and 0.0107 μm, respectively.

The mineralogical characteristics and phases of investigated ore-samples were determined using PANAnalytical Empyrean X-ray Diffractometer (MCL) with a Cu-Kα (λ = 0.1540 nm) radiation source operated at 45 kV and 40 mA, measurement of XRD pattern were performed from 5° to 90° 2theta range. The diffractograms obtained were interpreted using X'Pert HighScore Plus (version 4.6a (4.6.1.23823)). The quantitative elemental compositions of the ore-samples were determined using the PerkinElmer Optima 8000 ICP-OES. The elemental analysis was performed at different spectral emission lines using RF Power of 1500W with a Plasma and pump flow rate of 14.0 L/min, and 1.5 ml/min, respectively. The SEM attached with energy-dispersive x-ray spectroscopy (EDS) was also used for elemental analysis of the tantalum-tin containing ore-samples.

Five standard solutions were used to prepare solutions for calibrating Inductively coupled plasma-optical emission spectroscopy (ICP-OES). Three of the standard solutions were single element with each solution containing 1000 μg/mL of the elements U, Th, and Cs, respectively while the fourth and the fifth solutions were multi-elements containing 100 μg/mL of Ta, Nb, Ti, Sn, W, Zr and Si, and 1000 mg/L of Mn, Fe, Li, and Mg, respectively.

The standard solutions were prepared by mixing appropriate volumes of all the metal stock standard solutions and diluting the mixture with an appropriate volume of 2% nitric acid to make a total volume of 15 ml. From this solution, calibration solutions with concentrations of 10.0, 1.0, 0.1, and 0.01 ppm were prepared and 2% nitric acid was used as blank solution.

2.3. Sample preparation and characterization

The sampled ores were crushed, and ground to finer size of 125 μm using a ball mill. After grinding, the ore powder obtained were mixed thoroughly, and a representative sample was taken for physico-chemical and mineralogical characterization. The bulk density, tapped density, Carr's compressibility index (C) and Hausner ratio (H) were determined to get some information about powder properties and inter-particulate interactions in the studied samples. These interactions influence the bulk properties of the powder material and its flow due to the mechanical overlapping and interlocking of rock fragments [27,28]. The bulk and tap densities determination were carried out by filling the ore-sample into a graduated cylinder and weighing the mass of ore and its corresponding volume. The ratio of the mass to the volume obtained gives the value of the bulk density of the material. The tapped density was calculated after tapping mechanically the graduated cylinder containing the powdered ore-sample at least 125 taps and allowing it to fall under its own mass until the smallest final volume is obtained [29,30]. The compressibility index (C) and Hausner ratio (H) of the different samples were determined using Eqs. (1) and (2)

$$C = 100(1 - \rho_B / \rho_T) \quad (1)$$

$$H = \rho_T / \rho_B \quad (2)$$

where ρ_B and ρ_T are the powder's bulk and tapped densities respectively [30].

A table of flowability characteristics based on values of C and H was used to compare and evaluate the flowability of the ore-samples studied [31]. The samples for ICP-OES characterization were prepared by fusing in furnace at 1000 °C a mixture of the ore (0.1 g) with (1.0 g) of fluxing material (lithium tetraborate) in graphite crucible. After 1 h of heating, the melt was immediately dissolved in 25% nitric acid and stirred at room temperature for almost 1h30 min. To ensure a complete dissolution of all elements, a small amount (1.5 ml) of concentrated hydrofluoric acid was added. Then, 1.5 ml of the dissolved sample solution were taken and diluted 10 times with 2% nitric acid to obtain 15 ml of analytical solution [32].

3. Results and discussions

3.1. Physical properties

Physical properties used to study and describe the ore mineral samples (powder) include particle size distribution, densities and interparticle voids interactions. The inter-particle interactions influence the bulk properties of the powder material and its flow due to the overlapping and interlocking of rock fragments [27]. Rock density is an important source of information required for mineral resource and ore reserve estimation such as the ore tonnage and mineralization grades

Table 1
Bulk, Tap Densities, Carr's Index and Hausner Ratio for the different samples.

Sample	Mass (g)	Bulk volume (cm^3)	Tapped volume (cm^3)	Bulk Density ($g.cm^{-3}$)	Tapped Density ($g.cm^{-3}$)	Carr's index (%)	Hausner ratio
R–N1	17.54	25	16.50	0.701	1.063	34.05	1.51
R–N2	18.69	25	17.00	0.747	1.099	32.02	1.47
R–N3	16.68	25	17.00	0.667	0.981	32.00	1.47
R-KMY Raw	17.56	25	16.00	0.702	1.097	36.00	1.56
R-KMY Con	76.40	25	22.50	3.056	3.395	9.98	1.11

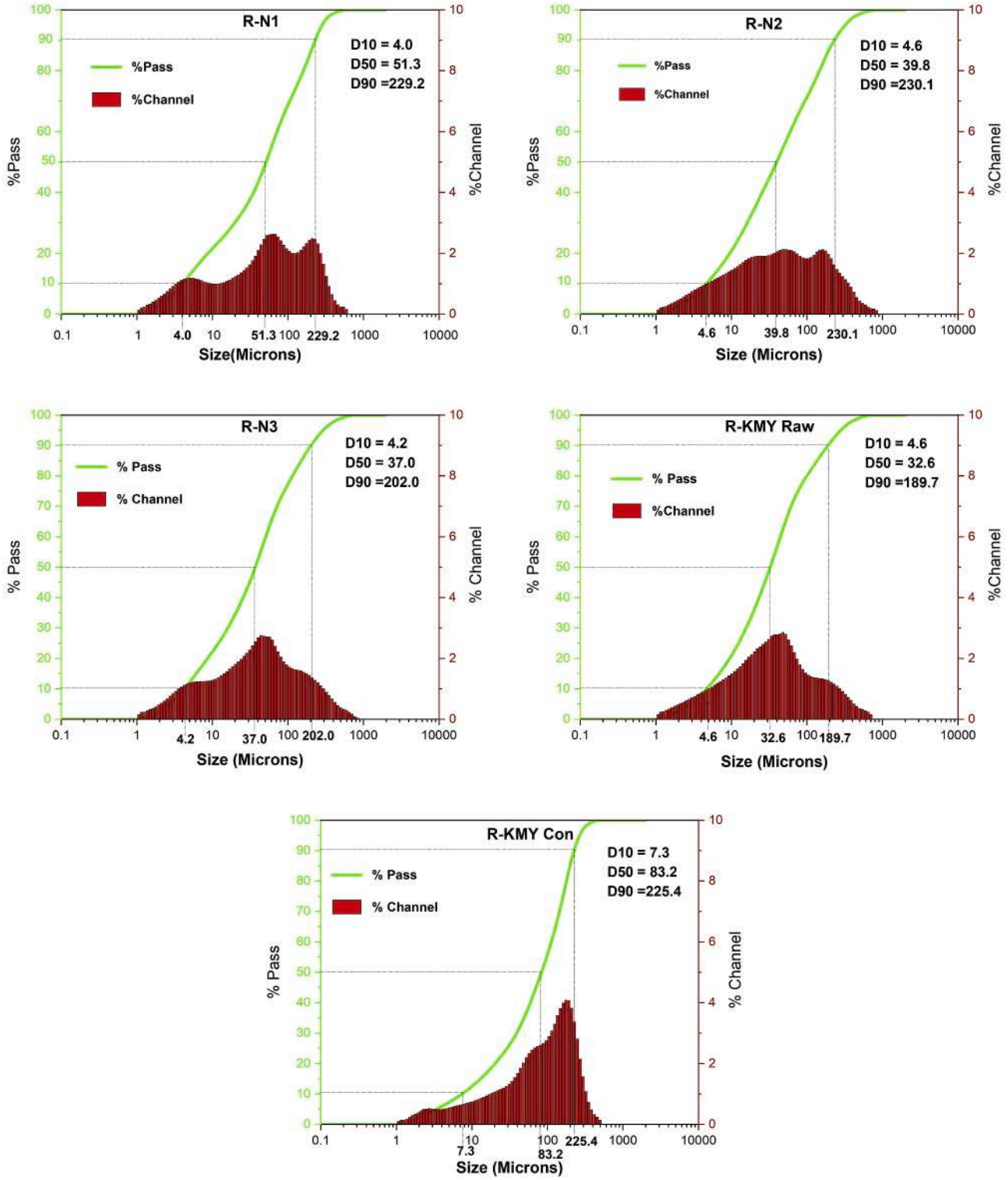

Fig. 3. Particle size distribution of samples R–N1, R–N2, R–N3, and R-KMY Con.

Table 2
Size classification of investigated ore-samples.

Sample	Total mass (g)	Sieve size (μm)	Mass retained (g)	Percentage retained (wt%)
R–N1	1062.59	355	210.79	19.83
		250	359.31	33.81
		125	492.49	46.34
R–N2	1199.71	355	110.43	9.20
		250	149.92	12.50
		125	939.39	78.30
R–N3	1514.52	355	124.25	8.20
		250	450.94	29.78
		125	939.33	62.02
R-KMY	1019.68	355	185.75	18.22
		250	639.07	62.67
		125	194.86	19.11

[33–35]. The bulk density of a rock is defined as the total mass of dried rock sample to its volume [36]. Since powders and granules are composed of particles and voids, bulk densities of free-flowing powders and granular substances depend on their texture, mineralogy, mass, particle shape and size distribution, and handling practices [37]. For a given mass, higher bulk densities indicate the powder compactness state, increased strength and lack of powder structure whereas lower bulk density indicates higher coarse-fragments content [27,38].

In order to get some insights on the inter-particulate voids interactions and to assess the flow properties of the different ore samples, we determined their bulk and tapped densities. Fig. 2 shows the comparison between bulk and tapped densities of the investigated ore samples. From the figure, sample R-KMY Con has the largest bulk and tap densities implying that the inter-particulate voids interactions are lesser than those in R–N1, R–N2 and R–N3. This increase in densities is attributed to the fact that the R-KMY Con has heavy particles with different sizes and shapes, thus higher volume when packed compared to the rest of the samples. We also determined the Hausner ratio and Carr's compressibility index from the bulk and tapped densities to understand the flowability characteristics of the samples. The C and H values of all the raw samples; R–N1, R–N2 and R–N3; range from 32.00 to 36.00 and from 1.47 to 1.56 respectively, showing that the particles are likely to be fine and spherical, thus the samples have poor flowability or good cohesive character [31]. The C and H values for the sample R-KMY Con are 9.98 and 1.11 which indicate that the sample has excellent flowability; the particles are mainly heavy, large size and irregular shapes, thus increased volume. The values of bulk density, tapped density, C and H for the different samples are summarized in Table 1.

The particle size distributions indicate the range size in which particles of minerals with commercial value are likely to be concentrated. The particle size distributions of the ore-samples were evaluated using the particle size analyzer, the Microtrac flowSync, and the results obtained are expressed as log-normal distributions as depicted in Fig. 3. From the figure, the particle size distribution for sample R–N1 showed a multi-modal distribution where 10% of the total volume of particles have diameters smaller than 4.05 μm, 50% have diameters smaller than 51.35 μm and 90% have diameters below 229.20 μm. Sample R–N2 displays a bimodal distribution where 10% of the particles have diameters less than 4.67 μm, 50% have diameters smaller than 39.83 μm and 90% of the particles have diameter lower than 230.10 μm. Samples R–N3 and R-KMY Raw showed normal particle distributions with 10%, 50% and 90% of the particles having diameters which are respectively less than 4.20, 37.0, 202.0, and 4.60, 32.60, 189.70 μm. The sample R-KMY Con showed a negatively skewed particle size distribution with one peak. The particle sizes are distributed in such way that 10% have diameters below 7.60 μm, 50% below 83.20 and 90% less than 225.40 μm. From the analysis, we see that samples R–N1 and R–N2 have more coarse-grained particles.

To get more understanding on the particle size distribution of the ore-samples, the samples were sieved and classified into different size fractions from 355 to 125 μm; as presented in Table 2; and each fraction obtained were beneficiated by gravity concentration to reduce the amount of gangue materials, mostly the light alumino-silicates minerals. The feed and concentrate obtained were taken for further characterization using ICP-OES. From Table 2, it is seen that the valuable minerals are likely to be located within the fraction with the highest percentage retained (wt%), 125 μm.

Table 3
ICP-OES Results of the studied ore-samples before size classification and beneficiation.

Oxides (%)	R-TN1	R-TN2	R-TN3	R-KMY Raw	R-KMY Con
Ta_2O_5	0.063	0.039	0.042	0.057	4.594
Nb_2O_5	0.062	0.050	0.057	0.062	2.666
Fe_2O_3	0.242	0.440	0.194	0.769	1.357
MnO	0.178	0.080	0.160	0.1860	1.420
MgO	0.124	0.133	0.103	0.113	0.653
SnO_2	0.256	0.067	0.088	0.469	53.443
WO_3	0.055	0.052	0.046	0.046	0.372
TiO_2	0.093	0.139	0.073	0.109	0.666
CaO	0.118	0.092	0.085	0.104	0.381
SiO_2	22.858	22.474	21.304	30.370	10.130
Al_2O_3	31.620	20.421	22.909	18.046	3.139
Na_2O	0.361	0.310	0.296	0.434	1.295
ZrO	0.054	0.054	0.051	0.056	0.446
ThO_2	0.083	0.086	0.100	0.098	0.095
U_3O_8	0.160	0.116	0.148	0.121	0.076

3.2. Chemical and mineralogical studies

The major elements associated with tantalum, which mostly contribute to the physical characteristics of the containing minerals, dictate the suitable method for its beneficiation [22]. The ICP-OES analysis of the ore-samples revealed the presence of Ta, Nb, Mn, Fe, Sn, Mg, Ti, U, Th, O among others. These elements are mainly dominated by Fe and Nb followed by Mn, Sn and Mg which are the main components of tantalite, columbite and cassiterite minerals. These elements were then expressed as oxides to reflect their natural occurrence in the investigated samples and the results are presented in Table 3.

From Table 3, compositions of tantalum and niobium oxides in the raw samples R–N1, R–N2, R–N3, and R-KMY Raw were almost the same. The highest levels of Ta_2O_5 and Nb_2O_5 were 0.063 wt% and 0.062 wt% respectively in sample R–N1, while the lowest concentrations were 0.039 wt% and 0.050 wt% in samples R–N2. The percentage weights of Ta_2O_5 and Nb_2O_5 increased from 0.057 to 0.062 to 4.594 and 2.666 in samples R-KMY Raw and R-KMY Con respectively. The results further showed an appreciable concentration of tin oxide ranging from 0.067 wt % to 0.469 wt% in samples R–N2 and R-KMY Raw respectively. In all ore-samples, concentration of Sn is higher than that of Ta and Nb, and concentration of Nb and Fe is higher than that of Ta and Mn. This means that the main mineral with commercial value in the ore-samples is cassiterite associated with particles of columbite-(Fe). The highest concentration of tin oxide 53.44 wt% associated with tantalite-(Mn) (4.59 wt% Ta_2O_5 and 1.42 wt% MnO) was observed in the concentrate R-KMY Con.

Radioactive elements such as thorium and uranium were also detected in trace amount below the critical value of 0.5 wt% in all ore-samples. All investigated ore-samples have almost similar mineralogical compositions, however sample R-KMY Raw showed higher concentrations of most elements analyzed except for aluminium. This may be due to the variations in mineralization of vein deposits hosting these minerals.

To further understand the mineralogy of the samples, we beneficiated the ore-samples by gravity concentration to reduce the gangue materials. The feed and concentrate obtained were characterized by ICP-OES to know their chemical compositions and the results are presented

Table 4
Results of ICP-OES Characterization of the Feed in different sizes.

Sample	Size (μm)	Feed composition (%)						
		Ta	Nb	Fe	Mn	Sn	Si	Al
R–N1	355	0.026	0.043	0.402	0.058	0.014	24.48	19.49
	250	0.0064	0.010	0.367	0.0484	0.042	9.406	19.24
	125	0.0143	0.016	0.400	0.075	0.082	9.887	20.70
R–N2	355	0.008	0.008	0.630	0.0456	0.074	40.393	8.428
	250	0.027	0.030	0.795	0.060	0.183	36.87	11.41
	125	0.004	0.014	1.151	0.088	0.059	7.434	20.47
R–N3	355	0.010	0.016	0.267	0.051	0.048	7.317	13.73
	250	0.010	0.016	0.406	0.060	0.064	7.905	18.07
	125	0.013	0.020	0.367	0.082	0.064	7.684	17.50
R-KMY	355	0.033	0.015	1.068	0.053	0.152	33.55	9.93
	250	0.013	0.025	1.270	0.060	0.228	9.876	10.44
	125	0.007	0.017	1.468	0.093	0.276	6.276	10.32

Table 5
Results of ICP-OES Characterization of the Concentrate in different sizes.

Sample	Size (μm)	Concentrate composition (%)						
		Ta	Nb	Fe	Mn	Sn	Si	Al
R–N1	355	2.527	2.143	0.378	0.773	52.094	10.44	2.30
	250	4.178	3.226	1.544	1.215	41.486	10.639	3.14
	125	6.279	4.831	1.235	1.896	33.340	4.052	2.65
R–N2	355	2.717	2.839	5.299	1.201	19.939	26.601	5.01
	250	2.273	2.320	5.907	1.000	23.254	26.419	2.46
	125	3.932	3.571	5.044	1.576	40.128	3.152	0.876
R–N3	355	3.937	4.755	1.689	1.740	48.798	8.238	1.30
	250	4.960	5.388	2.273	2.001	23.531	11.937	1.47
	125	4.538	4.909	2.865	1.825	22.625	14.4	1.79
R-KMY	355	4.55	1.75	3.78	0.82	41.75	15.43	1.73
	250	3.94	1.45	2.84	0.71	35.34	10.55	1.53
	125	3.38	1.17	2.35	0.60	37.75	9.20	1.24

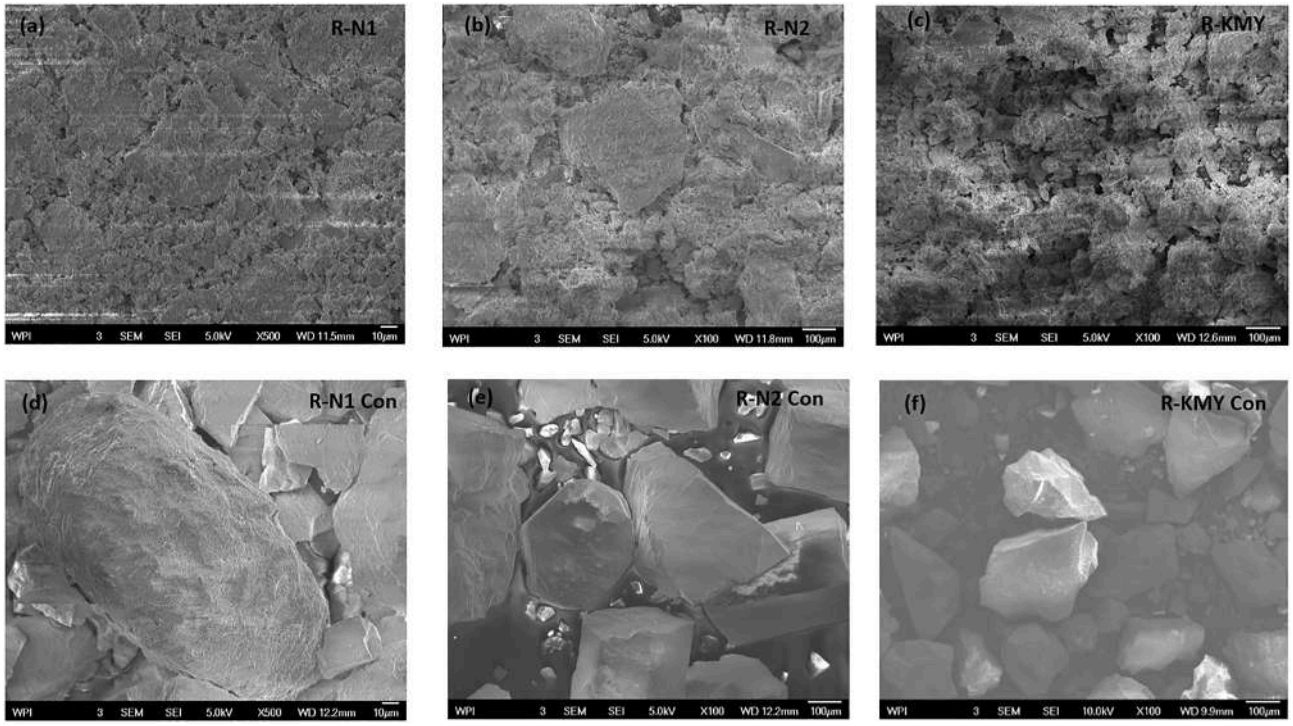

Fig. 4. SEM images of the raw (a, b, c) and concentrated ore-samples (d, e, f).

in Tables 4 and 5. In the feed (Table 4), most of the minerals with commercial value are concentrated in the size of 125 and 250 μm. In the concentrate portion (Table 5), particles of valuable minerals such as those of Ta, Nb, Fe and Mn are concentrated in the size of 125 μm except for the samples R–N3 and R-KMY where they are more retained in the size of 250 μm and 355 μm respectively. Tin in form of cassiterite; which

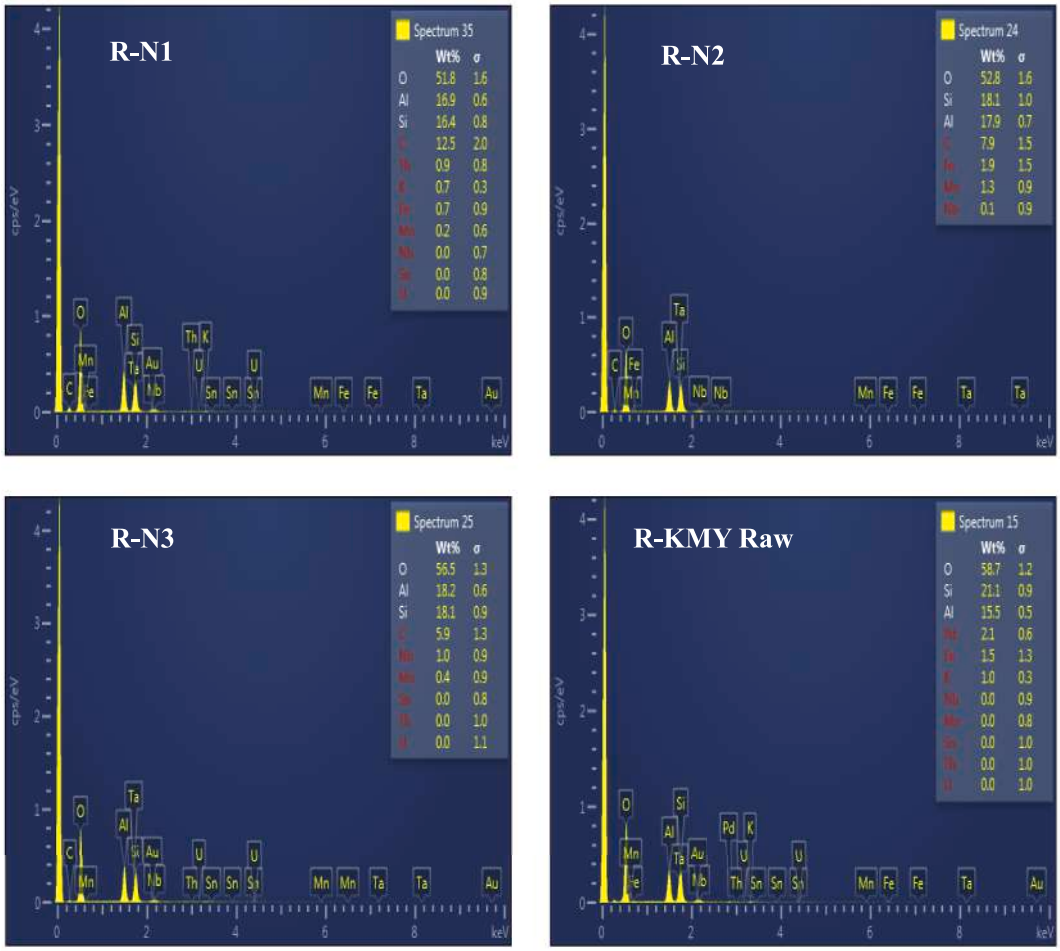

Fig. 5. EDS Spectra of the ore-samples before beneficiation.

is the main mineral; is concentrated within the size of 355 μm except for sample R–N2 where it is concentrated within 125 μm along with Ta, Nb, and Fe.

Howevers, in both the feed and the concentrate, concentration of Sn is higher than that of either Ta or Nb. In the feed, the percentage content of Nb and Fe is higher than that of Ta and Mn respectively for most of the fraction sizes. The highest amount of Fe and Nb in the concentrate is 5.90 wt% and 5.38 wt% respectively in samples R–N2 and R–N3 while for Ta the value is 6.27 wt% in sample R–N1. With exception of sample R–N1, Mn content is always lower than that of Fe. These facts make samples R–N2 and R–N3 to be columbite-(Fe) while R–N1 is tantalite-(Mn) as later confirmed by XRD analysis. The percentage of silicon and aluminium in form of kaolinite and muscovite which are the main components of the gangue materials, they are significantly reduced in the concentrate.

3.3. SEM-EDS results

A representative portion was taken from the raw samples R–N1, R–N2 and R-KMY Raw and their concentrates for SEM-EDS analysis to know their surface characteristics and elemental compositions, the results are depicted in Fig. 4. The SEM image of raw samples (a, b, c) demonstrates surface morphology characterized by coarse particles of different shapes and sizes on which the very fine particles are stacked and create a rough surface with porous structures. The morphology of the concentrate (d, e, f) is described by granular structure of particles of larger sizes with compact and smooth surface. This means that most of the gangue minerals were removed from the particle surface leaving larger and heavier particles, thus the grade of valuable minerals increased as determined in the semi-quantitative EDS.

The semi-quantitative EDS analysis of the ore-samples investigated in their raw forms, indicated that the surface composition is predominated with O, Si, and Al (Fig. 5) which confirm the presence of quartz, kaolinite and muscovite phases as further indicated by the XRD analysis (Fig. 7). The percentages of elements with commercial value such as tantalum, niobium, tin, and iron were very low, and some were not even detected. However, after beneficiation which reduced the gangue minerals mainly silicon and aluminium, the percentage composition of these valuable elements was increased, and mostly dominated by tin, niobium and iron as presented in Fig. 6. From the figure, it is evident that tin in form cassiterite is the main mineral of commercial value present in all samples, although samples R–N2 and R-KMY displayed in addition good signal columbite-(Fe).

3.4. XRD analysis

Fig. 7 present a comparison of XRD patterns of the ore-samples studied in their raw forms. From the figure, the diffractograms of all the ore-samples were found to have similar characteristic peaks with minor differences in intensities. Relative to the rest of the samples, R-KMY showed diffraction patterns with smaller peak intensities. The analysis of the diffractograms of the samples revealed the presence of quartz, kaolinite, and muscovite minerals, though quartz was not detected in sample R–N2. These minerals are usually found in placer deposits of pegmatite rocks resulting from deep weathering of igneous rocks and are also known to harbor some valuable minerals such as tin,

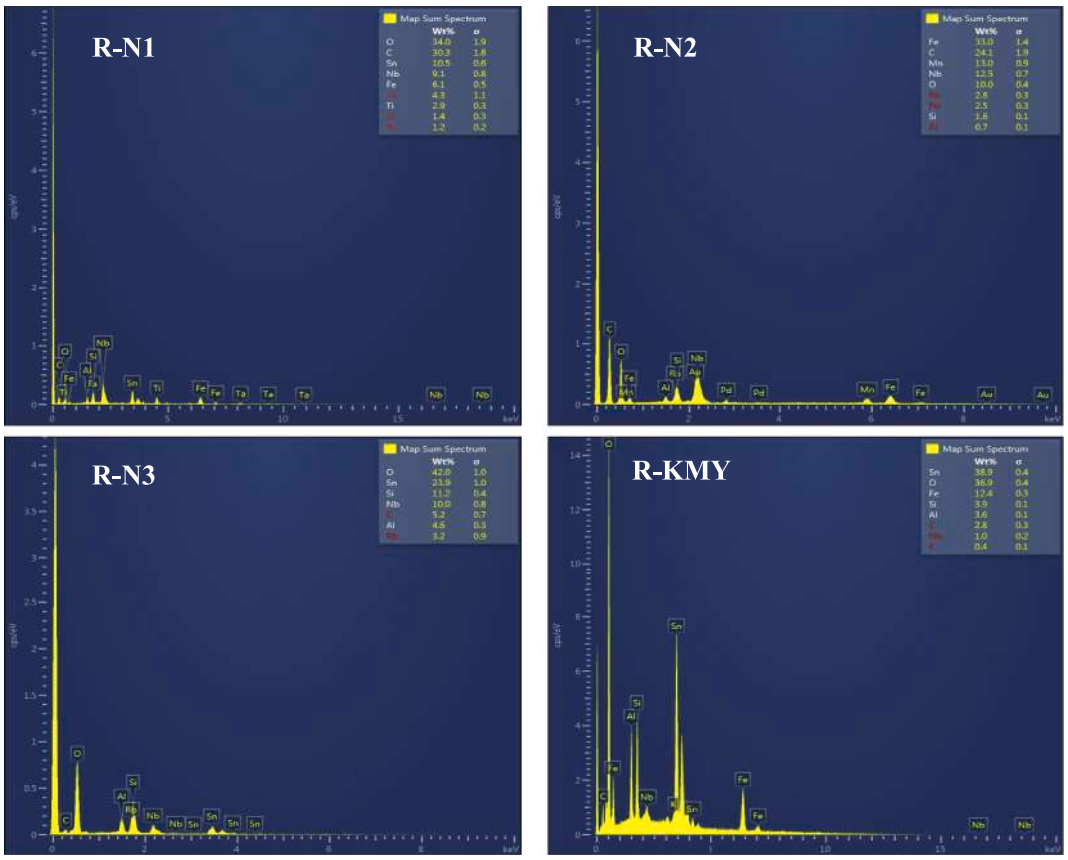

Fig. 6. EDS Spectra of ore-samples after beneficiation.

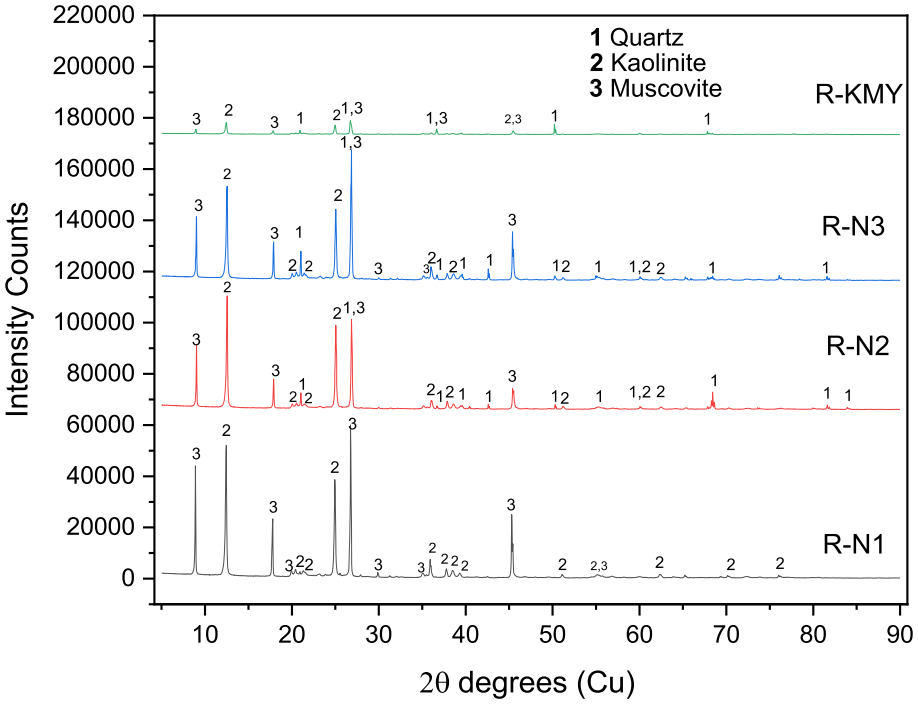

Fig. 7. XRD Pattern of ore-samples (Minerals in Raw Form).

tantalum, iron, niobium and manganese [39–41].

The peaks corresponding to the valuable minerals such as cassiterite, columbite, and tantalite were not visible possibly because they were masked by other peaks from the gangue. To figure out the presence of these minerals, we carried out XRD analysis of the concentrated portion of the samples, and the results are presented in Figs. 8 and 9. The XRD pattern of samples R–N1 and R–N2 showed almost similar characteristic peaks with minor differences in peak intensities. The analysis of these

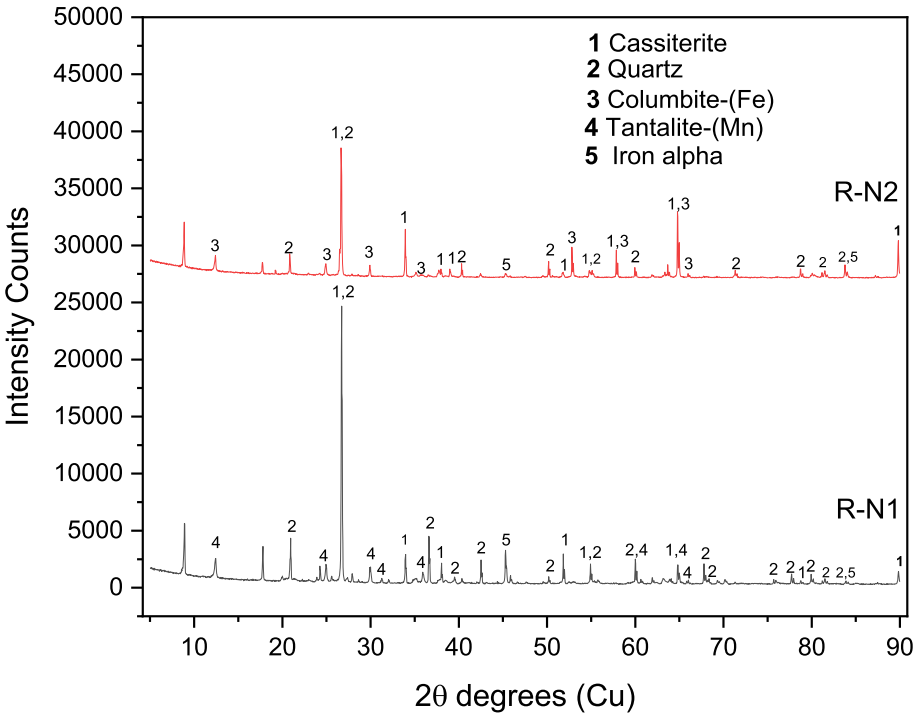

Fig. 8. XRD Pattern of samples R–N1 and R–N2 after beneficiation.

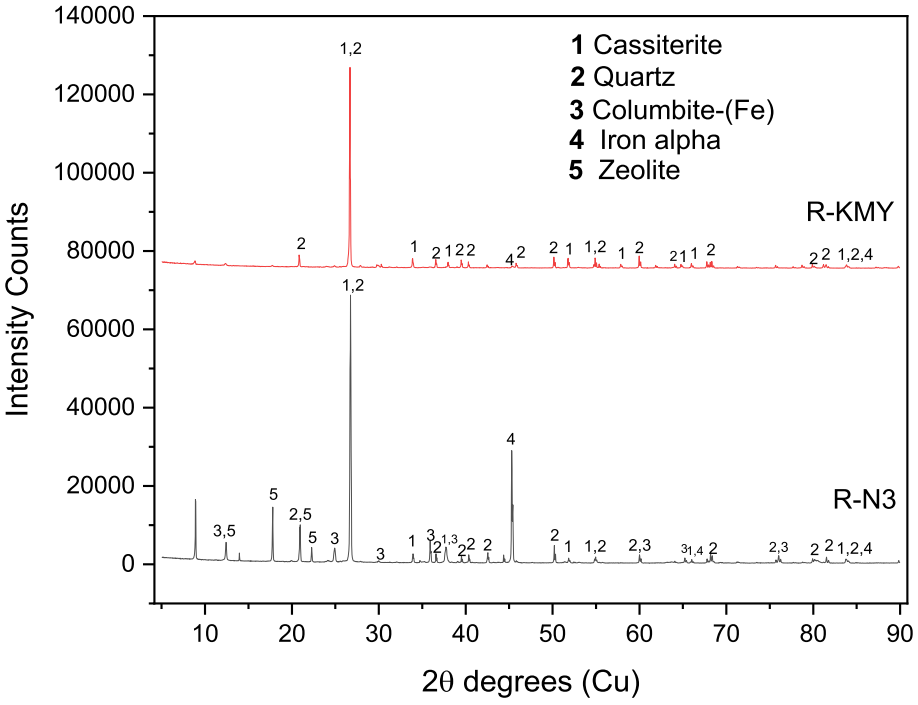

Fig. 9. XRD Pattern of samples R–N3 and R-KMY after beneficiation.

peaks revealed that the main constituent phases are cassiterite associated with tantalite-(Mn) and columbite-(Fe) minerals with minor peaks of quartz. The diffractogram of samples R–N3 and R-KMY presented in Fig. 9 showed distinctive peaks with those of sample R–N3 corresponding mainly to columbite-(Fe) and alpha iron hosted in zeolite and quartz phases. The diffraction peaks in sample R-KMY mainly correspond to cassiterite and quartz minerals. This observation agrees with the results of ICP-OES characterization (Table 4).

The presence of high concentration of light minerals such as quartz and alumino-silicates (specific gravity~2.8) and the heavy minerals such as cassiterite and columbite-(Fe) allows the ore-samples to be concentrated by gravity and magnetic separation as a possible beneficiation route. The observed differences in composition of valuable minerals of the studied ore-samples could be explained in terms of the diversity in mineralization of the ore deposits from site to site and from vein to vein [22], and mainly to the fact that niobium and tantalum can substitute each other freely in their minerals, the same situation also exists for iron and manganese [42].

4. Conclusion

The present study investigated physico-chemical and mineralogical characteristics, and compositions of tantalum-tin minerals in the ore-samples collected from different locations in Rwanda (Ntunga and Kamonyi). The studies based on ICP-OES revealed that all the ore-samples investigated have nearly similar chemical and mineralogical compositions, except sample R-KMY Raw which showed higher concentrations of most elements analyzed. The XRD results confirmed the similarities with identical characteristic peaks of the main minerals of quartz, kaolinite, and muscovite, although minor variations in peak intensities were noticed. The elements such as iron, tin, tantalum, and niobium were detected in low quantities, but their grades increased upon beneficiation of the ore-samples. The main ingredient present was cassiterite in association with columbite-(Fe) and tantalite-(Fe) minerals. The ore-sample was classified as low-grade ore as it contained less than 0.1% Ta_2O_5 and Nb_2O_5, and non-radioactive as the percentage of radioactive oxides were below the critical value of 0.5%. Thus, it requires to under-go concentration processes before dissolution and chemical leaching. The gravity concentration done on the ore-samples resulted in concentrate with compositions of 66.14%SnO_2, 7.66% Ta_2O_5 and 7.70% Nb_2O_5. This study therefore provides the baseline data for the selection and designing the appropriate techniques to effectively harness the tantalum-tin minerals from the sampled areas.

Author Contribution

Jean Baptiste Habinshuti: Methodology, Writing – original draft preparation, Investigation. Jeanne Pauline Munganyinka: Visualization and formal analysis. Adelana R. Adetunji: Writing-review and editing. Brajendra Mishra: Supervision and Resources. Grace Ofori-Sarpong: Writing review and editing. Gbetoglo Charles Komadja: Formal analysis and interpreatation. Janvier Mukiza: Conceptualization and validation. Himanshu Tanvar: Investigation. Azikiwe Peter Onwualu: Writing-review and editing.

Declaration of competing interest

The authors declare that they have no known competing financial interests or personal relationships that could have appeared to influence the work reported in this paper.

Acknowledgement

The authors acknowledge the PASET and World Bank for financial support.

References

[1] F. Melcher, et al., Tantalum-(niobium-tin) mineralisation in African pegmatites and rare metal granites: constraints from Ta-Nb oxide mineralogy, geochemistry and U-Pb geochronology, Ore Geol. Rev. 64 (2015) 667–719, https://doi.org/10.1016/j.oregeorev.2013.09.003.
[2] J.F.P. Klaus, J. Schulz, Nadine M. Piatak, Niobium and Tantalum, 2017. Reston, vol. A.
[3] L.A.T. Espinoza, L.A. Tercero Espinoza, Case Study: Tantalum in the World Economy. History, Uses and Demand, University of Dundee, Research and Innovation Services, Dundee, 2012.
[4] M. Toure, G. Arrachart, J. Duhamet, S. Pellet-Rostaing, Tantalum and niobium selective extraction by alkyl-acetophenone, Metals (Basel) 8 (9) (Aug. 2018) 654, https://doi.org/10.3390/met8090654.
[5] D. Bleiwas, J. Papp, T. Yager, Shift in Global Tantalum Mine Production, 2000 – 2014, 2015, https://doi.org/10.3133/fs20153079. Usgs, vol. Fact Sheet, no. December.
[6] P, N. H, D.S. Muchez, Geological mapping and implications for Nb-Ta, Sn and W prospection in Rwanda, Bull. DES SEANCES L'ACADEMIE R. DES Sci. D'OUTRE-MER 60 (3–4) (2014) 515–530.
[7] M.O.H. Amuda, D.E. Esezobor, G.I. Lawal, "Adaptable technologies for life – cycle processing of tantalum bearing minerals, J. Miner. Mater. Char. Eng. 6 (1) (2007) 69–77, https://doi.org/10.4236/jmmce.2007.61006.
[8] E. Allain, N. Kanari, F. Diot, J. Yvon, Development of a process for the concentration of the strategic tantalum and niobium oxides from tin slags, Miner. Eng. 134 (2019) 97–103, https://doi.org/10.1016/j.mineng.2019.01.029, no. July.
[9] C.L. Briant, M.K. Banerjee, Refractory metals and alloys, in: Reference Module In Materials Science And Materials Engineering, Elsevier, 2016, pp. 8088–8095.
[10] C. Subramanian, A.K. Suri, B. Atomic, Recovery of niobium and tantalum from low grade tin slag - a hydrometallurgical approach, Environ. Waste Manag. (1998) 100–107.
[11] S. Richard, G. Kathryn, "Niobium–tantalum: definitions, mineralogy and deposits, Br. Geol. Surv. (2011) 1–27.
[12] United States Geological Survey, Mineral Commodity Summaries 2020, 2020.
[13] J. Jeangrand, COMPREHENSIVE STRATEGIC ANALYSIS OF THE TANTALUM INDUSTRY, Simon Fraser University, Burnaby, BC, Canada, 2005.
[14] N. Motlalepula, Separation and Purification of Niobium and Tantalum from Synthetic and Natural Compounds, 2013.
[15] R.L. Parker, M. Fleischer, Geochemistry of Niobium and Tantalum : A Review of the Geochemistry of Niobium and Tantalum and a Glossary of Niobium and Tantalum Minerals, 1968.
[16] T.M. Ahmed, Niobium and Tantalum Geochemistry and Industrial Applications, 2016.
[17] R. Shaw, K. Goodenough, Niobium–tantalum, Br. Geol. Surv. (2011).
[18] TIC, Tantalum stock price | TIC [Online]. Available: https://www.tanb.org/about-tantalum/tantalum-valuation-basis. (Accessed 29 September 2020).
[19] Lauren Wolfe, How Dodd-Frank Is Failing Congo – Foreign Policy, 02-Feb-2015 [Online]. Available: https://foreignpolicy.com/2015/02/02/how-dodd-frank-is-failing-congo-mining-conflict-minerals/. (Accessed 30 September 2020).
[20] REMBAR, Global Tantalum Production, Conflict Minerals and the U. S. Dodd-Frank Act – what You Should Know - Rembar Co, 27-Aug-2019 [Online]. Available: https://www.rembar.com/global-tantalum-production-the-u-s-dodd-frank-act-and-conflict-minerals-what-you-should-know/. (Accessed 29 September 2020).
[21] H.L. Shergold, Flotation in mineral processing., (CAMBRIDGE, U.K. JUL. 5-16, 1982), in: K.J. IVES (Ed.), Sci. BASIS Flot. PROC. NATO Adv. STUDY INST., 1984, pp. 229–287, https://doi.org/10.1007/978-94-009-6926-1_7. no. 75) (ISBN 90-247-2907–6).
[22] A.R. Adetunji, W.O. Siyanbola, I.I. Funtua, S.O.O. Olusunle, A. Afonja, O. O. Adewoye, Assessment of beneficiation routes of tantalite ores from key locations in Nigeria, J. Miner. Mater. Char. Eng. (2005), https://doi.org/10.4236/jmmce.2005.42008.
[23] M. Nete, F. Koko, T. Theron, W. Purcell, J.T. Nel, Primary beneficiation of tantalite using magnetic separation and acid leaching, Int. J. Miner. Metall. Mater. (2014), https://doi.org/10.1007/s12613-014-1022-6.
[24] A.A. Baba, F.A. Adekola, O.I. Dele-Ige, R.B. Bale, Investigation of dissolution kinetics of A Nigerian tantalite ore in nitric acid, J. Miner. Mater. Char. Eng. 7 (1) (2008) 83–95, https://doi.org/10.4236/jmmce.2008.71007.
[25] M. Nete, W. Purcell, J.T. Nel, Tantalite beneficiation through sequential separation of radioactive elements, iron and titanium by magnetic separation and acid leaching, in: Advanced Materials Research, 2014, https://doi.org/10.4028/AMR.1019.419.
[26] B.G. Gebreyohannes, V. del Rosario Alberto, A. Yimam, G. Woldetinsae, B. Tadesse, Alternative beneficiation of tantalite and removal of radioactive oxides from Ethiopian Kenticha pegmatite–spodumene ores, Int. J. Miner. Metall. Mater. (2017), https://doi.org/10.1007/s12613-017-1456-8.
[27] S. Mukhopadhyay, R.E. Masto, R.C. Tripathi, N.K. Srivastava, Application of soil quality indicators for the phytorestoration of mine spoil dumps, in: Phytomanagement Of Polluted Sites: Market Opportunities In Sustainable Phytoremediation, Elsevier, 2018, pp. 361–388.
[28] J. Clayton, An introduction to powder characterization, in: Handbook Of Pharmaceutical Wet Granulation: Theory And Practice In a Quality By Design Paradigm, Elsevier, 2018, pp. 569–613.
[29] M. Honarpour, et al., Bulk density and tapped density of powders, World Health Org. XXXIII (2) (2012) 81–87.
[30] U.S.P.C. USPC, Method II-measurement in a volumeter, United States Pharma. Conv. 6 (2012) 2014–2016, 2014.
[31] D. W, Usama M. Attia, Andrew Fones, Ross Trepleton, Hugh Hamilton, Susan Davies, HIPing of Pd-doped titanium components: a study of mechanical and corrosion properties, in: 11th Int. Conf. Hot Isostatic Press, 2014 (HIP '14), no. January.
[32] A. Delijska, T. Blazheva, L. Petkova, L. Dimov, Fusion with lithium borate as sample preparation for ICP and AAS analysis, Fresenius' Z. für Anal. Chem. 332 (4) (Jan. 1988) 362–365, https://doi.org/10.1007/BF00468816.
[33] M.Z. Abzalov, Measuring and modelling of dry bulk rock density for mineral resource estimation, Trans. Institutions Min. Metall. Sect. B Appl. Earth Sci. 122 (1) (2013) 16–29, https://doi.org/10.1179/1743275813Y.0000000027.
[34] S.K. Haldar, Exploration geophysics, in: Mineral Exploration, Elsevier, 2018, pp. 103–122.
[35] M. Makhuvha, R.M. Arellano, D.M.W. Harney, Determination of bulk density, methods and impacts, with a case study from Los Bronces Mine, Chile, Trans. Institutions Min. Metall. Sect. B Appl. Earth Sci. 123 (3) (Sep. 2014) 196–205, https://doi.org/10.1179/1743275814Y.0000000058.
[36] P. Blistan, S. Jacko, Ľ. Kovanič, J. Kondela, K. Pukanská, K. Bartoš, Tls and sfm approach for bulk density determination of excavated heterogeneous raw materials, Minerals 10 (2) (Feb. 2020) 174, https://doi.org/10.3390/min10020174.
[37] A. Scogings, Bulk Density : Neglected but Essential, 2015, pp. 1–3, no. April.

[38] M.F. Hossain, W. Chen, Y. Zhang, "Bulk density of mineral and organic soils in the Canada's arctic and sub-arctic, Inf. Process. Agric. 2 (3–4) (2015) 183–190, https://doi.org/10.1016/j.inpa.2015.09.001.

[39] A. Goodship, A. Dace, P. O'Hare, J. Uwiringiyimana, R. Siddle, C. Moon, Geology and genesis of the Musha-Ntunga Sn-Ta-Li-Nb vein-pegmatite deposit, Rwanda: first results from deep drilling of a coltan mine in Rwanda and first detailed description of Li minerals, B. Appl. Earth Sci. 128 (2) (Apr. 2019) 47–48, https://doi.org/10.1080/25726838.2019.1602953.

[40] I. B. O. L. Y. A. I. A. N. U. M. U. Szegediensis, Acta U N I V E R S I T a T I S S Z E G E D I E N S I S, vol. 1, 2003.

[41] E. Klosek-Wawrzyn, J. Malolepszy, P. Murzyn, Sintering behavior of kaolin with calcite, in: Procedia Engineering, vol. 57, 2013, pp. 572–582, https://doi.org/10.1016/j.proeng.2013.04.073.

[42] Inorganic Ventures, Sample preparation guides [Online]. Available: https://www.inorganicventures.com/sample-preparation-guide/samples-containing-niobium-or-tantalum. (Accessed 19 October 2020) https://www.inorganicventures.com/sample-preparation-guide/samples-containing-niobium-or-tantalum.